

Nonlinear Lattice Relaxation of Photoexcited Diplatinum-Halide Chain Compounds

Jun Ohara and Shoji Yamamoto

Division of Physics, Hokkaido University, Sapporo 060-0810, Japan

(Dated: 15 August 2005)

In order to reveal the relaxation mechanism of photogenerated charge-transfer excitations in quasi-one-dimensional halogen-bridged diplatinum complexes, we calculate the low-lying adiabatic potential energy surfaces of a one-dimensional extended Peierls-Hubbard model. High-energy excitations above the electron-hole continuum may relax into polarons, while excitons pumped within the optical gap are self-localized and then either decay by luminescence or divide into solitons. Neutral solitons, charged solitons, and polarons may be simultaneously photogenerated in a diplatinum-halide chain, which has never been observed in any conventional platinum-halide chain. Optical conductivity is also simulated along the decay paths for experimental verification.

PACS numbers: 71.45.Lr, 78.20.Bh, 71.35.-y, 78.20.Ci

I. INTRODUCTION

Halogen (X)-bridged transition-metal (M) chain compounds, abbreviated as MX chains, have been attracting much interest for several decades. Substituting constituent metals, halogens, ligand molecules, and counter ions, we can widely tune their electronic structure and systematically study low-dimensional quantum phenomena in consequence of competing electron-electron (e-e) and electron-lattice (e-l) interactions.^{1,2} PtX chains, including Wolfram's red salt $[Pt(C_2H_7N)_4Cl]Cl_2 \cdot 2H_2O$,³ exhibit a Peierls-distorted mixed-valent ground state, whereas NiX chains, which are strongly correlated Mott insulators, have a monovalent regular-chain structure.⁴ Various ground⁵⁻⁷ and defect⁸⁻¹² states were theoretically predicted and indeed observed experimentally.¹³⁻²⁰ The photoinduced midgap absorption of $[Pt(C_2H_8N_2)_2Cl](ClO_4)_2$ caused a vigorous argument on self-trapped nonlinear excitations,²¹⁻²⁴ while the gigantic optical nonlinearity of $[Ni(C_6H_{14}N_2)_2Br]Br_2$ opened up a new way to optical devices.²⁵

The thus-fascinating MX family compounds have been gaining renewed interest in recent years due to their binuclear metal analogs,^{26,27} abbreviated as MMX chains, which exhibit quantum,²⁸⁻³⁰ thermal,³¹⁻³³ and pressure-induced³⁴⁻³⁷ transitions between a wider variety of mixed-valent states.^{38,39} The direct $M(d_{z^2})$ - $M(d_{z^2})$ overlap effectively reduces the on-site Coulomb repulsion and therefore makes electrons more itinerant. MMX chains are indeed much more conductive than MX chains.³¹ Then charge- and/or spin-carrying local excitations such as solitons⁴⁰ and polarons⁴¹ are more and more interesting. Thermally excited spin solitons have already been observed in $Pt_2(C_5H_{11}CS_2)_4I$.⁴² However, photogenerated MMX defect states have neither been measured nor been calculated yet. Effects of metal binucleation on the relaxation of photogenerated charge-transfer excitations are not only scientifically interesting in themselves but must be also the key to optical switching. Thus motivated, we simulate photoexcitation and nonlinear lattice relaxation of diplatinum-halide chains and stimulate further experimental explorations.

II. CALCULATIONAL PROCEDURE

We describe MMX chains by the one-dimensional $\frac{3}{4}$ -filled single-band Peierls-Hubbard adiabatic Hamiltonian

$$\begin{aligned} \mathcal{H} = & - \sum_{n,s} [t_{MXM} - \alpha(l_{n+1:-} + l_{n:+})] (a_{n+1,s}^\dagger b_{n,s} \\ & + b_{n,s}^\dagger a_{n+1,s}) - t_{MM} \sum_{n,s} (b_{n,s}^\dagger a_{n,s} + a_{n,s}^\dagger b_{n,s}) \\ & - \beta \sum_{n,s} (l_{n:-} n_{n,s} + l_{n:+} m_{n,s}) + \frac{K_{MX}}{2} \sum_n (l_{n:-}^2 \\ & + l_{n:+}^2) + U_M \sum_n (n_{n,\uparrow} n_{n,\downarrow} + m_{n,\uparrow} m_{n,\downarrow}) \\ & + \sum_{n,s,s'} (V_{MM} n_{n,s} m_{n,s'} + V_{MXM} n_{n+1,s} m_{n,s'}), \end{aligned} \quad (2.1)$$

where $n_{n,s} = a_{n,s}^\dagger a_{n,s}$ and $m_{n,s} = b_{n,s}^\dagger b_{n,s}$ with $a_{n,s}^\dagger$ and $b_{n,s}^\dagger$ creating an electron with spin s on the $M d_{z^2}$ orbitals in the n th MMX unit. t_{MM} and t_{MXM} give the intradimer and interdimer electron hoppings, respectively. α and β describe the Peierls- and Holstein-type e-l couplings, respectively, with K_{MX} being the metal-halogen spring constant. $l_{n:-} = v_n - u_{n-1}$ and $l_{n:+} = u_n - v_n$ with u_n and v_n being, respectively, the chain-direction displacements of the halogen and metal dimer in the n th MMX unit from their equilibrium positions. Every diplatinum moiety, with its surrounding ligands, is not deformed. The notation is further explained in Fig. 1. We take t_{MM} as twice t_{MXM} setting t_{MXM} and K_{MX} both equal to unity. Since the parameter sets (α, β, K_{MX}) and $(a\alpha, a\beta, a^2 K_{MX})$ are equivalent to each other with an arbitrary constant a , the specific value of K_{MX} is insignificant.⁴³ The number of MMX units, denoted by N , is set equal to 300.

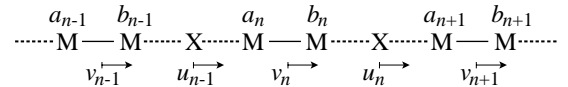


FIG. 1: Schematic representation of MMX chains.

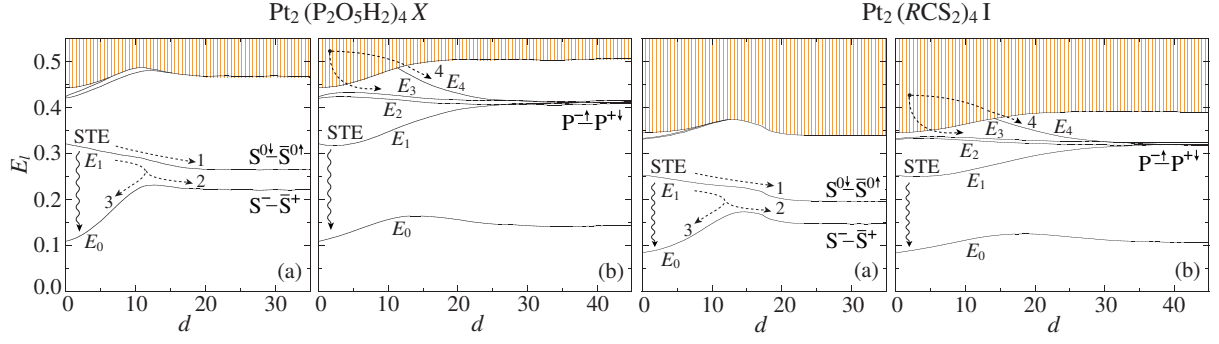


FIG. 2: (Color online) Adiabatic potential energies as functions of d measured from the ground-state energy. (a): Relaxation channels connected to soliton (S)-antisoliton ($\bar{\text{S}}$) pairs; (b): Relaxation channels connected to polaron (P) pairs. Dotted (wavy) arrows suggest possible relaxation paths (luminescence). $\alpha = 0.0, \beta = 1.2$ and $\alpha = 0.3, \beta = 0.8$ for the $\text{P}_2\text{O}_5\text{H}_2$ - and RCS_2 -ligand complexes, respectively; $U_M = 0.5$, $V_{MM} = 0.25$, and $V_{MXM} = 0.15$ in common.

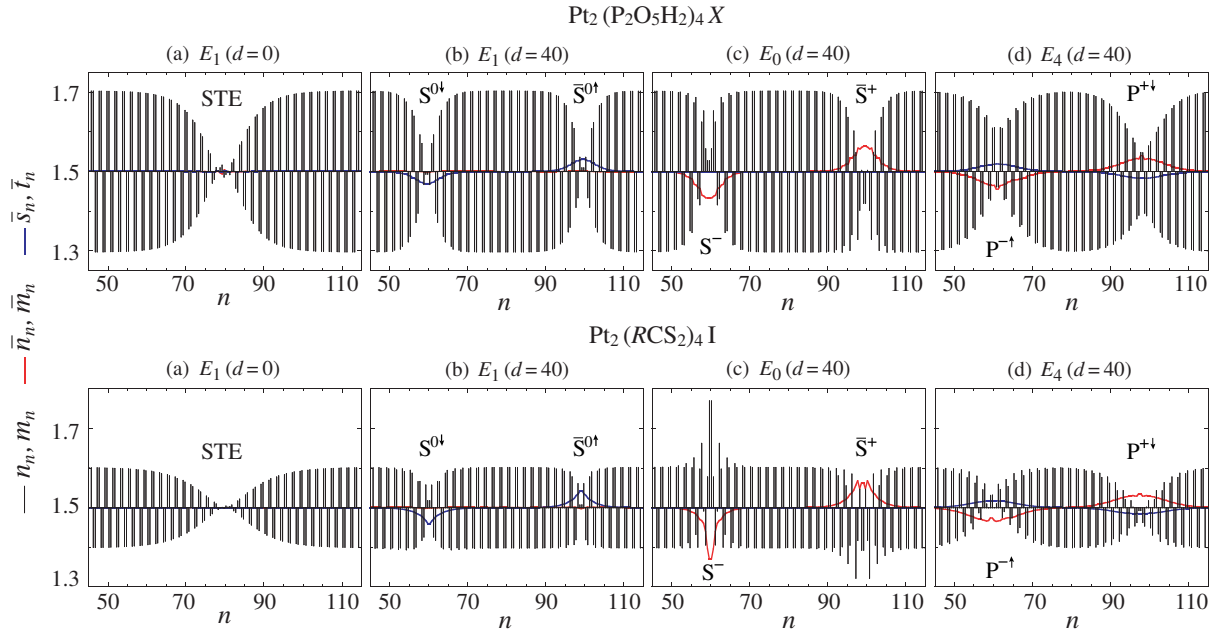


FIG. 3: (Color online) Spatial configurations of various photogenerated excitations. We first calculate the local electron ($\langle l|a_{n,\uparrow}^\dagger a_{n,\uparrow}|l\rangle + \langle l|a_{n,\downarrow}^\dagger a_{n,\downarrow}|l\rangle \equiv n_n$, $\langle l|b_{n,\uparrow}^\dagger b_{n,\uparrow}|l\rangle + \langle l|b_{n,\downarrow}^\dagger b_{n,\downarrow}|l\rangle \equiv m_n$) and spin ($\langle l|a_{n,\uparrow}^\dagger a_{n,\uparrow}|l\rangle - \langle l|a_{n,\downarrow}^\dagger a_{n,\downarrow}|l\rangle \equiv 2s_n$, $\langle l|b_{n,\uparrow}^\dagger b_{n,\uparrow}|l\rangle - \langle l|b_{n,\downarrow}^\dagger b_{n,\downarrow}|l\rangle \equiv 2t_n$) densities in the l th excited state and then extract their nonalternating components ($n_{n-1} + 2n_n + n_{n+1} \equiv -4\bar{n}_n$, $m_{n-1} + 2m_n + m_{n+1} \equiv -4\bar{m}_n$; $s_{n-1} + 2s_n + s_{n+1} \equiv 4\bar{s}_n$; $t_{n-1} + 2t_n + t_{n+1} \equiv 4\bar{t}_n$). In the above, the average electron density is added to the nonalternating components.

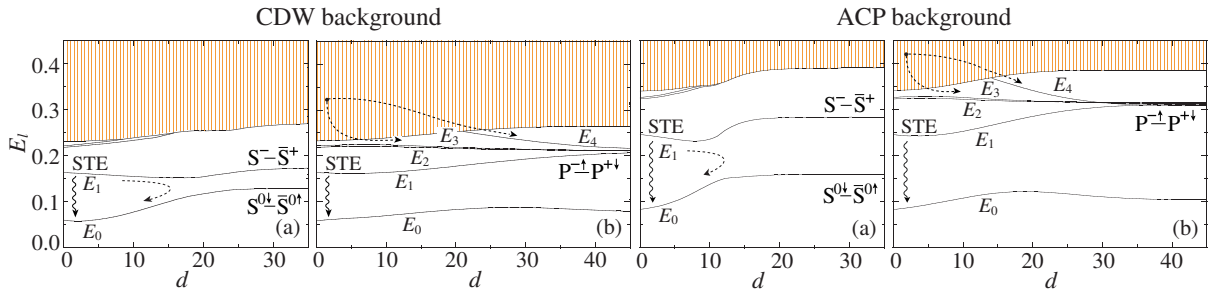


FIG. 4: (Color online) Adiabatic potential energies as functions of d measured from the ground-state energy. (a): Relaxation channels connected to soliton (S)-antisoliton ($\bar{\text{S}}$) pairs; (b): Relaxation channels connected to polaron (P) pairs. Dotted (wavy) arrows suggest possible relaxation paths (luminescence). $\alpha = 0.0, \beta = 1.2$ and $\alpha = 0.3, \beta = 0.8$ for the CDW and ACP backgrounds, respectively; $U_M = 1.0$, $V_{MM} = 0.5$, and $V_{MXM} = 0.3$ in common.

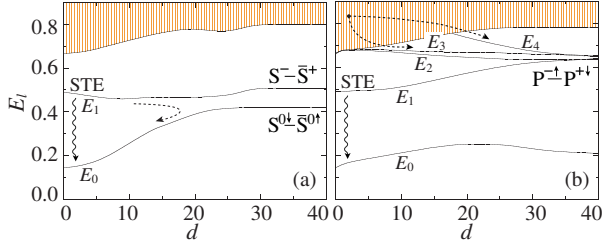


FIG. 5: (Color online) Adiabatic potential energies as functions of d measured from the ground-state energy in MX chains, where we employ the same type of Hamiltonian as Eq. (2.1) with $\alpha = 0.0$, $\beta = 0.7$, $U_M = 1.0$, and $V_{MXM} = 0.3$, which is relevant to $[\text{Pt}(\text{C}_2\text{H}_8\text{N}_2)_2\text{X}](\text{ClO}_4)_2$ ($X = \text{Cl}, \text{Br}$). (a): Relaxation channels connected to soliton (S)-antisoliton (\bar{S}) pairs; (b): Relaxation channels connected to polaron (P) pairs. Dotted (wavy) arrows suggest possible relaxation paths (luminescence).

The existent diplatinum-halide chain compounds are classified into two groups: $A_4[\text{Pt}_2(\text{P}_2\text{O}_5\text{H}_2)_4\text{X}] \cdot n\text{H}_2\text{O}$ ($X = \text{Cl}, \text{Br}, \text{I}$; $A = \text{Li}, \text{Cs}, \dots$)^{26,44} and $\text{Pt}_2(\text{RCS}_2)_4\text{I}$ ($R = \text{C}_n\text{H}_{2n+1}$).^{27,45} The former structurally resembles the MX conventional and exhibits a ground state with halogen-sublattice dimerization: $-\text{X}^- \dots \text{Pt}^{2+} \text{Pt}^{2+} \dots \text{X}^- - \text{Pt}^{3+} \text{Pt}^{3+} - \text{X}^- \dots$, which is referred to as the charge-density-wave (CDW) state, where the intrasite e-l coupling β is dominant. The latter possesses a distinct ground state with metal-sublattice dimerization, $\dots \text{I}^- \dots \text{Pt}^{2+} \text{Pt}^{3+} - \text{I}^- - \text{Pt}^{3+} \text{Pt}^{2+} \dots \text{I}^- \dots$, which is referred to as the alternate charge-polarization (ACP) state, where the intersite e-l coupling α is significant. Platinum-halide chains exhibit intermediate e-e interactions ($V_{MXM} \ll U_M \lesssim t_{MXM}$)^{2,9} and platinum binucleation should reduce the on-site repulsion. Thus the Pt_2X Coulomb parameters are, unless otherwise noted, set for $U_M = 0.5$, $V_{MM} = 0.25$, and $V_{MXM} = 0.15$. The e-l coupling constants are taken in two ways as $\alpha = 0.0, \beta = 1.2$ and $\alpha = 0.3, \beta = 0.8$, which are relevant to the $\text{P}_2\text{O}_5\text{H}_2$ - and RCS_2 -ligand complexes and indeed give the CDW and ACP ground states, respectively, under the above Coulomb parametrization.⁴⁶

Photogenerated charge-transfer excitations, spreading over the chain at first, are self-localized into excitons, solitons, and polarons.⁴ The whole relaxation scenario is describable with a trial wave function^{9,41,47}

$$l_{n;\pm} = (-1)^n l_0 \left[1 + \delta l \left(\tanh \frac{|n \pm \delta n| - d/2}{\sigma_n \xi} - 1 \right) \right], \quad (2.2)$$

where l_0 is set equal to the halogen-ion displacement in the uniformly distorted CDW ground state, while the rest of the variational parameters are determined so as to minimize the energy of the lowest-lying excited state. Once the CDW state is photoexcited into the Frank-Condon state, which still sits at $\delta l = 0$, the uniform bond alternation begins to be locally deformed. Increasing δl with d fixed to zero represents the self-localization of a charge-transfer exciton. The self-trapped exciton (STE) may

further divide into a pair of local defects with increasing d . There is also a possibility of a higher-energy pumped electron-hole (e-h) pair directly splitting into distant defects in a pair, with simultaneously increasing δl and d . ξ corresponds to the extent of a local defect, whereas δn allows the neighboring metal sites to behave unequally around the defect center. σ_n takes \pm according to relaxational channels. It is simply set equal to unity for solitonic defects, while it is defined as $\sigma_n = \text{sgn}(|n \pm \delta n| - d/2)$ for polaronic defects. In both cases, the key variable d indicates the interdefect distance. We optimize δl , ξ , and δn at each d .

With given $l_{n;\pm}$, we solve the Hartree-Fock (HF) Hamiltonian \mathcal{H}_{HF} and obtain the low-lying states $|l\rangle_{\text{HF}}$ of energy E_l^{HF} ($l = 0, 1, 2, \dots$). Then we consider refining the description of excited states, which may be generally given as

$$|l\rangle = \sum_s \sum_{\epsilon_{\mu,s} \leq \epsilon_F} \sum_{\epsilon_{\nu,s} > \epsilon_F} f(\mu, \nu, s; l) c_{\nu,s}^\dagger c_{\mu,s} |0\rangle_{\text{HF}}, \quad (2.3)$$

where ϵ_F is the Fermi energy and $c_{\lambda,s}^\dagger$ creates an electron with spin s in the λ th HF eigenstate of energy $\epsilon_{\lambda,s}$. The HF scheme describes any excited state as a single Slater determinant, that is, $f(\mu, \nu, s; l) = \delta_{\mu\nu s, l}$, taking no account of the residual interaction $\mathcal{H} - \mathcal{H}_{\text{HF}} \equiv \mathcal{V}$. Full diagonalization of \mathcal{H} on the basis of $|l\rangle$ must be the best way to deal with the excitonic effect. However, even at $N = 120$, for instance, such a calculation costs eight gigabyte memory and a hundred hours, which means spending more than a year in optimizing the wave function (2.2) at every fixed d . In an attempt to take the excitonic effect into calculation more efficiently, we may consider neglecting all the off-diagonal elements of \mathcal{V} and correcting the energy scheme perturbationally.⁹ Then the l th excited-state energy is expressed as $E_l = E_0 + \epsilon_{\nu,s} - \epsilon_{\mu,s} + {}_{\text{HF}}\langle l | \mathcal{V} | l \rangle_{\text{HF}}$, where $E_0 \equiv E_0^{\text{HF}}$. Such a perturbational treatment of the excitonic effect is not only practical but also fairly quantitative under the not-so-strong electronic correlation of our present interest. We have indeed confirmed for short chains that the thus-obtained energies E_l well approximate those of excited states of the configuration-interaction (CI) type (see Appendix A). This is not the case with strongly correlated nickel complexes.⁴⁸ The following variational calculation is carried out so as to minimize E_1 with respect to δl , ξ , and δn at each d . When we take particular interest in the l th energy surface, E_l may be minimized instead. However, the whole energy scheme is not sensitive to the variational target and remains unchanged visually.

III. ADIABATIC POTENTIAL ENERGY SURFACES

Figure 2 presents the thus-calculated energy surfaces, the left two of which are relevant to $A_4[\text{Pt}_2(\text{P}_2\text{O}_5\text{H}_2)_4\text{X}] \cdot n\text{H}_2\text{O}$, while the right two of

which are to $\text{Pt}_2(\text{RCS}_2)_4\text{I}$. The electron-hole continuum of $\text{Pt}_2(\text{RCS}_2)_4\text{I}$ lies lower in energy than that of $A_4[\text{Pt}_2(\text{P}_2\text{O}_5\text{H}_2)_4\text{X}] \cdot n\text{H}_2\text{O}$. In fact $\text{Pt}_2(\text{CH}_3\text{CS}_2)_4\text{I}$ exhibits much smaller optical gap than conventional MX chain compounds and even shows metallic conduction at room temperature.³¹ The relaxation channels of the $\text{P}_2\text{O}_5\text{H}_2$ - and RCS_2 -ligand complexes are qualitatively the same. Fully trapped excitons [Fig. 3(a)], unless decay by luminescence, are dissociated into soliton (S)-antisoliton ($\bar{\text{S}}$) pairs [Figs. 3(b) and 3(c)], whereas there is no possibility of their relaxing into polaron (P) pairs. $\text{P}^{-\uparrow} - \text{P}^{+\downarrow}$ pairs [Fig. 3(d)] may be created from higher-energy excited states. No energy barrier between an STE and any $\text{S} - \bar{\text{S}}$ pair, which is not the case with PtX chains,^{9,47} should result in very short decay time of STEs and long life time of $\text{S} - \bar{\text{S}}$ pairs. The soliton and antisoliton in any $\text{S} - \bar{\text{S}}$ pair have localized wave functions and their overlap rapidly decreases with increasing d . Therefore, instantaneous charge transport between far distant S and $\bar{\text{S}}$ is hardly probable and tunneling between the energy surfaces E_1 and E_0 is restricted to the region of moderately small d .

Under the relatively weak correlation relevant to Pt_2X chains, charged soliton pairs $\text{S}^- - \bar{\text{S}}^+$ are lower in energy than neutral soliton pairs $\text{S}^{0\downarrow} - \bar{\text{S}}^{0\uparrow}$.⁴⁹ Figures 3(b) and 3(c) show that solitons and antisolitons on the energy surface E_1 carry net spins, whereas those on the energy surface E_0 convey net charges. As the Coulomb repulsion grows, the polaronic channel qualitatively remains unchanged, while the solitonic one significantly varies. Figure 4 indeed shows that $\text{S}^- - \bar{\text{S}}^+$ pairs are possibly higher in energy than STEs as well as $\text{S}^{0\downarrow} - \bar{\text{S}}^{0\uparrow}$ pairs. Increasing on-site Coulomb repulsion reduces the Peierls gap, especially on the CDW background. Figure 4 is reminiscent of the situation in PtX chains,^{9,47} which is reproduced in Fig. 5. Photoinduced midgap absorption of $[\text{Pt}(\text{C}_2\text{H}_8\text{N}_2)_2\text{X}](\text{ClO}_4)_2$ ($\text{X} = \text{Cl}, \text{Br}$)^{18,20} was actually attributed to neutral solitons.^{4,47} In comparison with PtCl and PtBr chains, PtI chains have a larger supertransfer energy t_{MXM} (Ref. 1) and thus exhibit effectively suppressed e-e interactions. Consequently there appear charged solitons instead of neutral ones in photoexcited $[\text{Pt}(\text{C}_2\text{H}_8\text{N}_2)_2\text{I}](\text{ClO}_4)_2$.¹⁷ PtX compounds generally exhibit further absorption bands due to polarons within the gap,^{4,50} provided the excitation energy is higher than the charge-transfer gap Δ . However, there is no signal of neutral and charged solitons being simultaneously photogenerated in PtX chains, probably because either $\text{S}^{0\downarrow} - \bar{\text{S}}^{0\uparrow}$ or $\text{S}^- - \bar{\text{S}}^+$ pairs are necessarily higher in energy than STEs.⁴⁷ Figure 2 promises dramatic observations: *Neutral solitons, charged solitons, and polarons may be simultaneously detected in photoexcited diplatinum-halide chain compounds.* The decay time of luminescent STEs, τ , is a few hundred picoseconds in $[\text{Pt}(\text{C}_2\text{H}_8\text{N}_2)_2\text{Cl}](\text{ClO}_4)_2$,^{51,52} which is much shorter than the radiative lifetime and therefore comes from the dissociation to $\text{S}^{0\downarrow} - \bar{\text{S}}^{0\uparrow}$ pairs. In

$A_4[\text{Pt}_2(\text{P}_2\text{O}_5\text{H}_2)_4\text{X}] \cdot n\text{H}_2\text{O}$, the $\text{S}^{0\downarrow} - \bar{\text{S}}^{0\uparrow}$ path is likely open to an STE without any potential barrier in between and therefore STEs must decay still faster possibly with $\tau \ll 100$ ps.

IV. PHOTOINDUCED ABSORPTION SPECTRA

In order to encourage time-resolved optical measurements on Pt_2X chains, we calculate photoinduced absorption spectra as functions of the interdefect distance d . The real part of the optical conductivity on the potential energy surface E_l is represented as

$$\sigma(\omega) = \frac{\pi}{N\omega} \sum_{l'} |\langle l' | \mathcal{J} | l \rangle|^2 \delta(\tilde{E}_{l'} - E_l - \hbar\omega), \quad (4.1)$$

where the current operator $\mathcal{J} \equiv \sum_{n,s} j_{n,s}$ is given by

$$j_{n,s} = \frac{ie}{\hbar} c_{\text{MXM}} [t_{\text{MXM}} - \alpha(l_{n+1:-} + l_{n:+})] (a_{n+1,s}^\dagger b_{n,s} - b_{n,s}^\dagger a_{n+1,s}) + \frac{ie}{\hbar} c_{\text{MM}} t_{\text{MM}} (b_{n,s}^\dagger a_{n,s} - a_{n,s}^\dagger b_{n,s}), \quad (4.2)$$

with c_{MM} and c_{MXM} being the average M - M and M - X - M distances, respectively, and set for $c_{\text{MXM}} = 2c_{\text{MM}}$. When we take $|l\rangle_{\text{HF}}$ for $|l\rangle$ with the perturbationally corrected energy scheme E_l , we obtain $|l'\rangle = c_{\nu',s'}^\dagger c_{\mu',s'} |l\rangle_{\text{HF}}$ and $\tilde{E}_{l'} = E_l^{\text{HF}} + \epsilon_{\nu',s'} - \epsilon_{\mu',s'} + \langle l' | \mathcal{V} | l' \rangle$. Figures 6(a)–6(d) present the optical conductivity spectra along the relaxation paths labeled 1–4 in Fig. 2, where (a)–(c) are characteristic of solitonic excitations via STEs, while (d) of a polaronic one from the e-h continuum. The intra-gap absorption bands visualize various nonlinear lattice relaxation paths distinguishably, which are scaled up and interpreted in Fig. 7.

In Fig. 7(a), an STE splits into far distant $\text{S}^{0\downarrow}$ and $\bar{\text{S}}^{0\uparrow}$, while in Fig. 7(b), an STE relaxes into far distant S^- and $\bar{\text{S}}^+$ via quantum tunneling. In PtX chains, $\text{S}^- - \bar{\text{S}}^+$ pairs, instead of $\text{S}^{0\downarrow} - \bar{\text{S}}^{0\uparrow}$ pairs, lie in the same potential energy surface as STEs', but they can not be reached due to their high energy. Here in Pt_2X chains, STEs can nonradiatively decay into both neutral- and charged-soliton pairs and therefore the early decrease of their luminescence intensity should look double-exponential. The optical conductivity spectra are informative about the soliton charge. With increasing d , the exciton-to-band infrared absorption peak moves upward, whereas the intra-exciton midgap one downward. After passing each other, the former merges into the soliton-to-band absorption, while the latter fades out with S and $\bar{\text{S}}$ going away from and less overlapping with each other. Such a scenario is common to both $\text{S}^{0\downarrow} - \bar{\text{S}}^{0\uparrow}$ and $\text{S}^- - \bar{\text{S}}^+$ paths, but their long-time spectra look different. The neutral-soliton-to-band absorption spectrum consists of two close peaks and is thus broader than the charged-soliton-to-band one. For $\text{Pt}_2(\text{RCS}_2)_4\text{I}$, it is remarkably humped

FIG. 6: (Color online) Photoinduced absorption spectra along possible relaxation paths: (a) $\text{STE} \rightarrow \text{S}^{0\downarrow} - \bar{\text{S}}^{0\uparrow}$; (b) $\text{STE} \rightarrow \text{S}^- - \bar{\text{S}}^+$; (c) $\text{STE} \rightarrow \text{S} - \bar{\text{S}} \rightarrow \text{CDW}$; (d) $\text{e} - \text{h} \rightarrow \text{P}^{-\uparrow} - \text{P}^{+\downarrow}$.

due to the two intragap soliton levels lying relatively far apart from each other. On the ACP background, the intragap soliton levels are more sensitive to the e-e interactions.⁵³ $\text{Pt}_2(\text{RCS}_2)_4\text{I}$ exhibits another surviving absorption in the infrared region, which is attributable to the electron transfer between S and $\bar{\text{S}}$. This is because of larger ξ in $\text{Pt}_2(\text{RCS}_2)_4\text{I}$ (see Fig. 3). Solitons are more delocalized on the ACP background than on the CDW background. Figure 7(c) describes a nonradiative geminate recombination through the solitonic state, where the intra-exciton absorption peak turns upward and merges with the background interband absorption.

Figure 7(d) depicts polaronic excitations, which are efficiently generated through high-energy pumping. There are four potential energy surfaces leading to $\text{P}^{-\uparrow} - \text{P}^{+\downarrow}$ pairs. Although STEs lie in one of them, they have no chance of relaxing into polarons. When charge-transfer excitations split into polaron pairs, the intragap absorption spectra at small d , that is, the early observations, significantly vary with their relaxation paths, but they all converge to well-separated two bands. The intra-polaron absorption is higher in energy and stronger in intensity than the polaron-to-band one.

V. SUMMARY

We have calculated the nonlinear lattice relaxation paths of photogenerated charge-transfer excitations in diplatinum-halide chain compounds and “observed” their optical conductivity spectra. There is a possibility of *neutral solitons, charged solitons, and polarons coexisting in photoexcited Pt_2X chains* especially of the RCS_2 -ligand type, which is never the case with conventional PtX chains. The optical-conductivity spectra due to po-

laron pairs generally comprise well-separated two bands, while those due to soliton pairs mainly consist of a single band but its structure is rather varied with the ground state and the relaxation path. The S^- -to-band absorption is truly single-peaked, while the S^0 -to-band absorption gives a broader band with a shoulder in the lower-energy side. In $\text{Pt}_2(\text{RCS}_2)_4\text{I}$, the S-to- $\bar{\text{S}}$ absorption is long surviving and detectable in the infrared region in addition.

Indeed there are many similarities between the Pt_2X and PtX relaxation mechanisms, but their solitonic channels qualitatively differ. *In Pt_2X chains, both neutral- and charged-soliton paths are open to photogenerated charge-transfer excitons* and soliton pairs stably survive longer life time. The present study is motivated in part by the pioneering calculations on PtX chains,⁹ where no observable to be measured was presented, however. Nowadays, the time-resolved optical spectroscopy technique has been much more refined than before and the full spectrum can be analyzed with femtosecond precision.⁵⁴ Such circumstances have stimulated us to have the idea of calculating Fig. 6, spending a week on each run along the relaxation paths. Even the photoinduced midgap absorption of a prototypical platinum-halide chain compound $[\text{Pt}(\text{C}_2\text{H}_8\text{N}_2)_2\text{Cl}](\text{ClO}_4)_2$ ^{14,55} is not yet completely solved in spite of the enthusiastic argument.^{15,18,22,23,47} Diplatinum-halide chain compounds comprise two groups with distinct mixed-valent ground states and their electronic states are much more tunable. Comparative measurements, including photoinduced absorption, luminescence, and electron spin resonance, on the $\text{P}_2\text{O}_5\text{H}_2$ - and RCS_2 -ligand MMX complexes must reveal their intrinsic nonlinear lattice relaxation mechanism and may even give a key to unsettled issues on MX complexes.

FIG. 7: (Color online) The low-energy part of Fig. 6 is scaled up, together with the intragap level scheme and occupancy, where round arrows denote optically allowed excitations, while dotted arrows suggest tunneling between different energy surfaces.

Acknowledgments

The authors thank K. Iwano for fruitful discussions. This work was supported by the Ministry of Education, Culture, Sports, Science, and Technology of Japan.

APPENDIX A: COMPARISON BETWEEN THE HF AND CI SCHEMES

Adiabatic potential energies of short chains ($N = 50$) are calculated by the CI scheme (\times) as well as the per-

turbationally refined HF method (\circ) and are compared with Figs. 2(a) and 4(a) in Fig. 8.

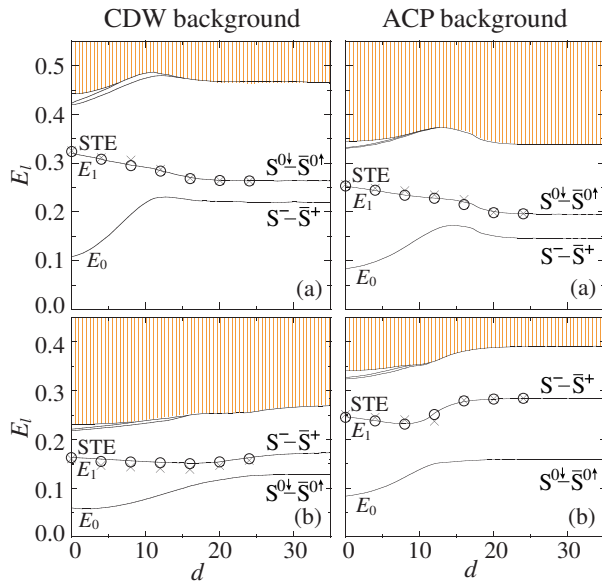


FIG. 8: (Color online) Relaxation paths leading to soliton (S)-antisoliton (\bar{S}) pairs. $\alpha = 0.0, \beta = 1.2$ and $\alpha = 0.3, \beta = 0.8$ for the CDW and ACP backgrounds, respectively. (a) $U_M = 0.5$, $V_{MM} = 0.25$, $V_{MXM} = 0.15$; (b) $U_M = 1.0$, $V_{MM} = 0.5$, $V_{MXM} = 0.3$.

- ¹ J. T. Gammel, A. Saxena, I. Batistić, A. R. Bishop, and S. R. Phillpot, Phys. Rev. B **45**, 6408 (1992).
- ² S. W. Weber-Milbrodt, J. T. Gammel, A. R. Bishop, and E. Y. Loh, Jr., Phys. Rev. B **45**, 6435 (1992).
- ³ H. Reihlen and E. Flohr, Ber. Dtsch. Chem. Ges. **67**, 2010 (1934).
- ⁴ H. Okamoto and M. Yamashita, Bull. Chem. Soc. Jpn. **71**, 2023 (1998).
- ⁵ I. Batistić, J. T. Gammel, and A. R. Bishop, Phys. Rev. B **44**, 13228 (1991).
- ⁶ H. Röder, A. R. Bishop, and J. T. Gammel, Phys. Rev. Lett. **70**, 3498 (1993).
- ⁷ S. Yamamoto, Phys. Lett. A **247**, 422 (1998); Synth. Met. **103**, 2683 (1999).
- ⁸ D. Baeriswyl and A. R. Bishop, J. Phys. C **21**, 339 (1988).
- ⁹ A. Mishima and K. Nasu, Phys. Rev. B **39**, 5758 (1989); *ibid.* **39**, 5763 (1989).
- ¹⁰ A. Mishima and K. Nasu, Phys. Rev. B **40**, 5593 (1989).
- ¹¹ I. Batistić and A. R. Bishop, Phys. Rev. B **45**, 5282 (1992).
- ¹² X. Z. Huang and A. R. Bishop, Phys. Rev. B **48**, R16148 (1993).
- ¹³ N. Kuroda, M. Sakai, Y. Nishina, M. Tanaka, S. Kurita, Phys. Rev. Lett. **58**, 2122 (1987).
- ¹⁴ S. Kurita, M. Haruki, and K. Miyagawa, J. Phys. Soc. Jpn. **57**, 1789 (1988).
- ¹⁵ R. J. Donohoe, S. A. Ekberg, C. D. Tait, and B. I. Swanson, Solid State Commun. **71**, 49 (1989).
- ¹⁶ M. Haruki and S. Kurita, Phys. Rev. B **39**, 5706 (1989).
- ¹⁷ H. Okamoto, T. Mitani, K. Toriumi, and M. Yamashita, Phys. Rev. Lett. **69**, 2248 (1992).
- ¹⁸ N. Kuroda, M. Ito, Y. Nishina, A. Kawamori, Y. Kadera, and T. Matsukawa, Phys. Rev. B **48**, 4245 (1993).
- ¹⁹ N. Kuroda, Y. Wakabayashi, M. Nishida, N. Wakabayashi, M. Yamashita, and N. Matsushita, Phys. Rev. Lett. **79**, 2510 (1997).
- ²⁰ H. Okamoto, Y. Kaga, Y. Shimada, Y. Oka, Y. Iwasa, T. Mitani, and M. Yamashita, Phys. Rev. Lett. **80**, 861 (1998).
- ²¹ J. T. Gammel, R. J. Donohoe, A. R. Bishop, and B. I. Swanson, Phys. Rev. B **42**, 10566 (1990).
- ²² M. Suzuki and K. Nasu, Phys. Rev. B **45**, 1605 (1992).
- ²³ K. Iwano and K. Nasu, J. Phys. Soc. Jpn. **61**, 1380 (1992).
- ²⁴ I. Batistić, X. Z. Huang, A. R. Bishop, and A. Saxena, Phys. Rev. B **48**, 6065 (1993).
- ²⁵ H. Kishida, H. Matsuzaki, H. Okamoto, T. Manabe, M. Yamashita, Y. Taguchi, and Y. Tokura, Nature **405**, 929 (2000).
- ²⁶ C.-M. Che, F. H. Herbstein, W. P. Schaefer, R. E. Marsh, and H. B. Gray, J. Am. Chem. Soc. **105**, 4604 (1983).
- ²⁷ C. Bellitto, A. Flamini, L. Gastaldi, and L. Scaramuzza, Inorg. Chem. **22**, 444 (1983).
- ²⁸ K. Marumoto, H. Tanaka, S. Kozaki, S. Kuroda, S. Miya, T. Kawashima, and M. Yamashita, Solid State Commun. **120**, 101 (2001).
- ²⁹ S. Yamamoto, Phys. Rev. B **63**, 125124 (2001).
- ³⁰ M. Kuwabara and K. Yonemitsu, J. Phys. Chem. Solids **62**, 435 (2001).
- ³¹ H. Kitagawa, N. Onodera, T. Sonoyama, M. Yamamoto, T. Fukawa, T. Mitani, M. Seto, and Y. Maeda, J. Am. Chem. Soc. **121**, 10068 (1999).
- ³² S. Ikeuchi, K. Saito, Y. Nakazawa, A. Sato, M. Mitsumi, K. Toriumi, and M. Sorai, Phys. Rev. B **66**, 115110 (2002).
- ³³ S. Yamamoto, J. Phys. Soc. Jpn. **70**, 1198 (2001).
- ³⁴ B. I. Swanson, M. A. Stroud, S. D. Conradson and M. H. Zietlow, Solid State Commun. **65**, 1405 (1988).
- ³⁵ H. Matsuzaki, T. Matsuoka, H. Kishida, K. Takizawa, H.

- Miyasaka, K. Sugiura, M. Yamashita, and H. Okamoto, Phys. Rev. Lett. **90**, 046401 (2003).
- ³⁶ H. Ito, Y. Hasegawa, H. Tanaka, S. Kuroda, M. Mitsumi, and K. Toriumi, J. Phys. Soc. Jpn. **72**, 2149 (2003).
- ³⁷ S. Yamamoto, Phys. Rev. B **64**, 140102(R) (2001).
- ³⁸ S. Yamamoto, Phys. Lett. A **258**, 183 (1999).
- ³⁹ M. Kuwabara and K. Yonemitsu, Mol. Cryst. Liq. Cryst. **341**, 533 (2000); *ibid.* **343**, 47 (2000).
- ⁴⁰ S. Yamamoto and M. Ichioka, J. Phys. Soc. Jpn. **71**, 189 (2002).
- ⁴¹ S. Yamamoto, Phys. Rev. B **66**, 165113 (2002).
- ⁴² H. Tanaka, S. Kuroda, T. Yamashita, M. Mitsumi, and K. Toriumi, J. Phys. Soc. Jpn. **72**, 2169 (2003).
- ⁴³ M. Kuwabara and K. Yonemitsu, J. Mater. Chem. **11**, 2163 (2001).
- ⁴⁴ R. J. H. Clark, M. Kurmoo, H. M. Dawes, M. B. Hursthouse, Inorg. Chem. **25** (1986) 409.
- ⁴⁵ S. Ikeuchi, K. Saito, Y. Nakazawa, M. Mitsumi, K. Toriumi, and M. Sorai, J. Phys. Chem. B **108**, 387 (2004).
- ⁴⁶ S. Yamamoto, J. Phys. Soc. Jpn. **69**, 13 (2000).
- ⁴⁷ K. Iwano, J. Phys. Soc. Jpn. **66**, 1088 (1997).
- ⁴⁸ J. Ohara and S. Yamamoto, J. Phys. Chem. Solids **66**, 1571 (2005).
- ⁴⁹ J. Ohara and S. Yamamoto, Phys. Rev. B **70**, 115112 (2004).
- ⁵⁰ R. J. Donohoe, L. A. Worl, C. A. Arrington, A. Bulou, and B. I. Swanson, Phys. Rev. B **45**, 13185 (1992).
- ⁵¹ H. Tanino, W. W. Rühle, and K. Takahashi, Phys. Rev. B **38**, R12716 (1988).
- ⁵² Y. Wada, U. Lemmer, E. O. Göbel, M. Yamashita, and K. Toriumi, Phys. Rev. B **52**, 8276 (1995).
- ⁵³ J. Ohara and S. Yamamoto, J. Phys. Soc. Jpn. **74**, 250 (2005).
- ⁵⁴ S. Iwai, M. Ono, A. Maeda, H. Matsuzaki, H. Kishida, H. Okamoto, and Y. Tokura, Phys. Rev. Lett. **91**, 057401 (2003).
- ⁵⁵ M. Sakai, N. Kuroda, and Y. Nishina, Phys. Rev. B **40**, 3066 (1989).

This figure "Fig6.jpg" is available in "jpg" format from:

<http://arxiv.org/ps/cond-mat/0512636v1>

This figure "Fig7.jpg" is available in "jpg" format from:

<http://arxiv.org/ps/cond-mat/0512636v1>